

RESEARCH

Open Access



Predicting drug response of tumors from integrated genomic profiles by deep neural networks

Yu-Chiao Chiu¹, Hung-I Harry Chen^{1,2}, Tinghe Zhang², Songyao Zhang^{2,3}, Aparna Gorthi¹, Li-Ju Wang¹, Yufei Huang^{2,4*} and Yidong Chen^{1,4*}

From The International Conference on Intelligent Biology and Medicine (ICIBM) 2018
Los Angeles, CA, USA. 10-12 June 2018

Abstract

Background: The study of high-throughput genomic profiles from a pharmacogenomics viewpoint has provided unprecedented insights into the oncogenic features modulating drug response. A recent study screened for the response of a thousand human cancer cell lines to a wide collection of anti-cancer drugs and illuminated the link between cellular genotypes and vulnerability. However, due to essential differences between cell lines and tumors, to date the translation into predicting drug response in tumors remains challenging. Recently, advances in deep learning have revolutionized bioinformatics and introduced new techniques to the integration of genomic data. Its application on pharmacogenomics may fill the gap between genomics and drug response and improve the prediction of drug response in tumors.

Results: We proposed a deep learning model to predict drug response (DeepDR) based on mutation and expression profiles of a cancer cell or a tumor. The model contains three deep neural networks (DNNs), i) a mutation encoder pre-trained using a large pan-cancer dataset (The Cancer Genome Atlas; TCGA) to abstract core representations of high-dimension mutation data, ii) a pre-trained expression encoder, and iii) a drug response predictor network integrating the first two subnetworks. Given a pair of mutation and expression profiles, the model predicts IC₅₀ values of 265 drugs. We trained and tested the model on a dataset of 622 cancer cell lines and achieved an overall prediction performance of mean squared error at 1.96 (log-scale IC₅₀ values). The performance was superior in prediction error or stability than two classical methods (linear regression and support vector machine) and four analog DNN models of DeepDR, including DNNs built without TCGA pre-training, partly replaced by principal components, and built on individual types of input data. We then applied the model to predict drug response of 9059 tumors of 33 cancer types. Using per-cancer and pan-cancer settings, the model predicted both known, including EGFR inhibitors in non-small cell lung cancer and tamoxifen in ER+ breast cancer, and novel drug targets, such as vinorelbine for *TTN*-mutated tumors. The comprehensive analysis further revealed the molecular mechanisms underlying the resistance to a chemotherapeutic drug docetaxel in a pan-cancer setting and the anti-cancer potential of a novel agent, CX-5461, in treating gliomas and hematopoietic malignancies.

(Continued on next page)

* Correspondence: Yufei.Huang@utsa.edu; ChenY8@uthscsa.edu

²Department of Electrical and Computer Engineering, The University of Texas at San Antonio, San Antonio, TX 78249, USA

¹Greehey Children's Cancer Research Institute, University of Texas Health Science Center at San Antonio, San Antonio, TX 78229, USA

Full list of author information is available at the end of the article



(Continued from previous page)

Conclusions: Here we present, as far as we know, the first DNN model to translate pharmacogenomics features identified from in vitro drug screening to predict the response of tumors. The results covered both well-studied and novel mechanisms of drug resistance and drug targets. Our model and findings improve the prediction of drug response and the identification of novel therapeutic options.

Keywords: Deep neural networks, Pharmacogenomics, Drug response prediction, Cancer cell line encyclopedia, Genomics of Drug Sensitivity in Cancer, The Cancer Genome Atlas

Background

Due to tumor heterogeneity and intra-tumor sub-clones, an accurate prediction of drug response and an identification of novel anti-cancer drugs remain challenging tasks [1, 2]. Pharmacogenomics, an emerging field studying how genomic alterations and transcriptomic programming determine drug response, represents a potential solution [3, 4]. For instance, recent reports identified mutation profiles associated with drug response both in tumor type-specific and pan-cancer manners [5, 6]. As drug response data of large patient cohorts are scarcely available, large-scale cell line-based screening can greatly facilitate the study of pharmacogenomics in cancer. Recently, the Genomics of Drug Sensitivity in Cancer (GDSC) Project proposed a comprehensively landscape of drug response of ~1000 human cancer cell lines to 265 anti-cancer drugs and unveiled crucial oncogenic aberrations related to drug sensitivity [7, 8]. Because of the fundamental differences between in vitro and in vivo biological systems, a translation of pharmacogenomics features derived from cells to the prediction of drug response of tumors is to our knowledge not yet realized.

Deep learning (DL) is the state-of-the-art machine learning technology for learning knowledge from complex data and making accurate predictions. It features the ability to learn the representation of data without the need for prior knowledge and an assumption on data distributions. The DL technology has been successfully applied to bioinformatics studies of regulatory genomics, such as predicting binding motifs [9], investigating DNA variants [10], deciphering single-cell omics [11, 12], and extraction of genomics features for survival prediction [13]. In pharmaceutical and pharmacogenomics research, reports have shown its ability to predict drug-target interactions [14], screen for novel anti-cancer drugs [15], and predict drug synergy [16]. Nevertheless, data complexity and the requirement of large training datasets have limited its application to integrate genomics data and comprehensively predict drug response, hindering the translation to precision oncology.

Addressing the unmet demands, the present study is aimed to predict the response of tumors to anti-cancer

drugs based on genomic profiles. We designed DeepDR, a deep neural network (DNN) model to learn the genetic background from high-dimensional mutation and expression profiles using the huge collection of tumors of The Cancer Genome Atlas (TCGA). The model was further trained by the pharmacogenomics data developed in human cancer cell lines by the GDSC Project and their corresponding genomic and transcriptomic alterations, and finally applied to TCGA data again to predict drug response of tumors. Collectively, DeepDR is a novel DL model that translates cell line-derived pharmacogenomics knowledge via tumor genomic and transcriptomic abstraction to predict tumors' response to compound treatment.

Methods

Datasets

We downloaded gene-level expression data of 935 cell lines of the Cancer Cell Line Encyclopedia (CCLE) and 11,078 TCGA pan-cancer tumors from the CTD² Data Portal [17] and UCSC TumorMap [18], respectively. Given the total numbers of cell lines, tumors, and genes as C , T , G , respectively, we metricized the expression data by $E^{CCLE} = \{ \log_2(tpm_{g,c}^{CCLE} + 1) \}$, where $tpm_{g,c}^{CCLE}$ is the number of transcripts per million of gene g ($g \in [1, G]$) in cell line c ($c \in [1, C]$), and $E^{TCGA} = \{ \log_2(tpm_{g,t}^{TCGA} + 1) \}$, where $tpm_{g,t}^{TCGA}$ denotes the number of transcripts per million of the same gene in tumor t ($t \in [1, T]$). Genes with low information burden (mean < 1 or st. dev. < 0.5) among TCGA samples were removed. Mutation Annotation Format (MAF) files of mutation data were downloaded directly from CCLE (1463 cells) [19, 20] and TCGA databases (10,166 tumors). Here we only considered four types of nonsynonymous mutations, including missense and nonsense mutations, and frameshift insertions and deletions. Thus, we had binary matrices of $M^{CCLE} = \{ m_{g,c}^{CCLE} \}$ and $M^{TCGA} = \{ m_{g,t}^{TCGA} \}$, where $m_{g,c}^{CCLE}$ and $m_{g,t}^{TCGA}$ are the mutation states (1 for mutation and 0 for wildtype) of gene g in c and t , respectively. Genes with no mutations in CCLE and TCGA samples were eliminated.

We also downloaded drug response data of 990 CCLE cell lines to 265 anti-cancer drugs measured by the half maximal inhibitory concentration (IC_{50}) from the GDSC Project [7]. IC_{50} were measured in μM and represented in log scale (i.e., $IC^{CCLE} = \{ \log_{10}(ic_{d,c}^{CCLE}) \}$, with d denoting the d -th drug and $d \in [1, D]$) and missing data were imputed by a weighted mean of IC_{50} of 5 nearest drugs using R packages VIM and laeken [21, 22]. In this study, we analyzed 622 cell lines with available expression, mutation, and IC_{50} data and 9059 tumors with expression and mutation profiles.

General settings of DNNs and computation environment

DNN training in this study were performed using the python library Keras 1.2.2 with TensorFlow backend. We used fully (or densely) connected layers for all networks. At a neuron j , its output y_j is calculated by

$$y_j = F\left(\sum_i w_{ij}x_i + b_j\right) \tag{1}$$

, where x_i is the output of neuron i at the previous layer of j , w_{ij} and b_j denote the synaptic weight and bias, respectively, and F represents an activation function. The notation of all neurons at a layer can thus be written as

$$\mathbf{y} = F(\mathbf{w}\mathbf{x} + \mathbf{b}). \tag{2}$$

During training, synaptic weights and biases are adjusted to minimize a loss function. We hereafter refer to the two parameters as synaptic parameters because they represent the model and can be used to transfer a learned model to another. In this study, DNNs were optimized using the Adam optimizer with a loss function of mean squared error (MSE). We used the He’s uniform distribution [23] to initialize autoencoders and the Prediction (P) network, while the mutation encoder (M_{enc}) and expression encoder (E_{enc}) in the complete model were initialized by the synaptic parameters learned from the pre-training on TCGA data. Neuron activation function was set as rectified linear unit (ReLU) except for the output layer of P as linear in order to better fit the distribution of log-scale IC_{50} .

Overview of DeepDR

DeepDR was developed to predict IC_{50} values based on genomic profiles of a cell or a tumor. Given the pair of mutation and expression vectors of sample c , $\{M^{CCLE}(:, c), E^{CCLE}(:, c)\}$, the model predicts a D -length vector of IC_{50} , $\widehat{IC}^{CCLE}(c)$, as an output. As shown in Fig. 1, the model is composed of three networks: i) a mutation encoder (M_{enc}), ii) an expression encoder (E_{enc}), and iii) a prediction feedforward network (P). The first and second components are the encoding parts of two

autoencoders pre-trained using TCGA data to transform high-order features of mutation and expression data into a lower dimensional representation. The encoded representations of mutation and expression profiles were linked into P and the entire model was trained on CCLE data to make prediction of IC_{50} values. Details of DeepDR are described below.

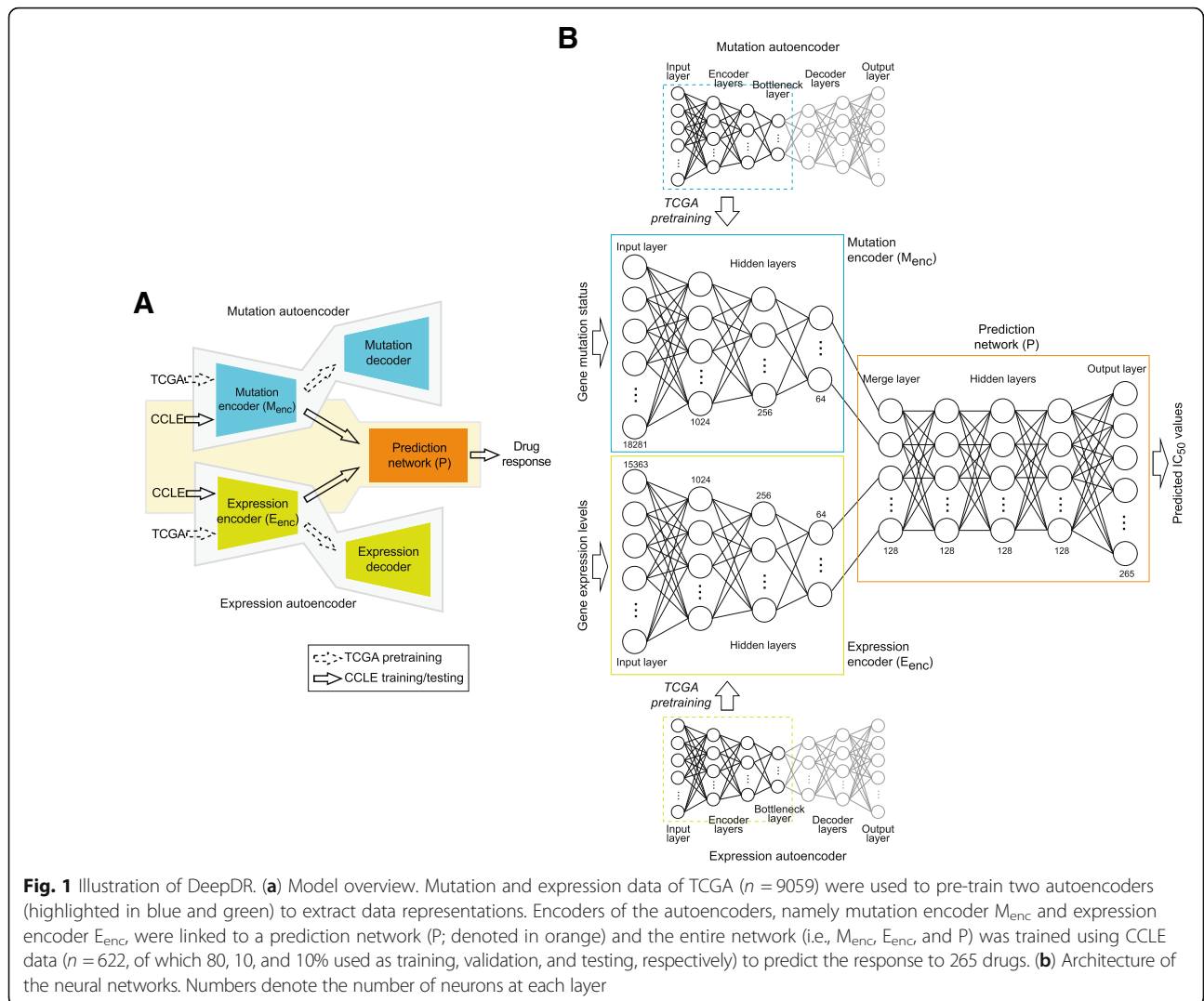
Pre-training of mutation and expression encoders

Autoencoder is an unsupervised DL architecture that includes a symmetric pair of encoder and decoder. By minimizing the loss between input and reconstructed (i.e., decoded) data, it reduces the dimension of complex data and captures crucial features at the bottleneck layer (the layer between encoder and decoder) (Fig. 1b, top and bottom panels). We pre-trained an autoencoder on each of the TCGA mutation and expression datasets to optimize the capability to capture high-order features. To determine the optimized architecture, we adopted a hyper-parameter optimization method, namely hyperas [24], to select i) number of neurons at the 1st layer (4096, 2048, or 1024), ii) number of neurons at the 2nd layer (512, 256, or 128), iii) number of neurons at the 3rd layer (the bottleneck layer; 64, 32, or 16), and iv) batch size (128 or 64). Each combination was trained for 20 epochs; the best-performing model was re-run for 100 epochs and the synaptic parameters were saved.

Complete prediction network

In our complete model, encoders of the two optimized autoencoders, i.e., M_{enc} and E_{enc} , were linked to P to make predictions of IC_{50} (Fig. 1). P is a 5-layer feed-forward neural network, including the first layer merging output neurons of the two encoders, three fully connected layers, and the last layer of D neurons generating IC_{50} values of D drugs (Fig. 1b, orange box). In the complete model, architecture (number of layers and number of neurons at each layer) of M_{enc} and E_{enc} was fixed; their synaptic parameters were initialized using the parameters obtained from pre-training in TCGA and updated during the training process. P was randomly initialized. We trained the entire model using CCLE data, with 80, 10, and 10% of samples as training, validation, and testing sets, respectively. We note the validation dataset was not used to update model parameters but to stop the training process when the loss in validation set had stopped decreasing for 3 consecutive epochs to avoid model overfitting. Performance of the model was evaluated using the testing samples, i.e., $MSE(\widehat{IC}^{CCLE}(:, C_{test}), IC^{CCLE}(:, C_{test}))$, where C_{test} denotes the test set of cell lines.

We applied the final model to predict drug response of TCGA tumors. For a tumor t , $\{M^{TCGA}(:, t), E^{TCGA}(:, t)\}$



was fed into the model and $IC_{50}^{TCGA}(\cdot, t)$ was calculated. A high predicted IC_{50} indicates an adverse response of a patient to the corresponding drug.

Comparison to other model designs

Performance of DeepDR was compared to four different DNN designs. First, to assess the effect of TCGA pre-training on M_{enc} and E_{enc} , we randomly initialized both encoders using the He’s uniform distribution and calculated MSE of the entire model. Second, dimension reduction of the M_{enc} and E_{enc} networks was replaced by principal component analysis (PCA). Last two models were built without M_{enc} or E_{enc} to study whether they jointly improved the performance. In each iteration, CCLE samples were randomly assigned to training (80%), validation (10%), and testing (10%) and each model was trained and tested. Performance in terms of the number of consumed epochs and MSE in IC_{50} were

summarized and compared across the 100 iterations. We also analyzed two classical prediction methods, multivariate linear regression and regularized support vector machine (SVM). For each method, top 64 principal components of mutations and gene expression were merged to predict IC_{50} values of all (using linear regression) or individual drugs (SVM).

Results

Construction and evaluation of DeepDR in CCLE

The study is aimed to predict drug response (measured as log-scale IC_{50} values) using genome-wide mutation and expression profiles. We included mutation and expression profiles of 622 CCLE cell lines of 25 tissue types and 9059 TCGA tumors of 33 cancer types. After data preprocessing, 18,281 and 15,363 genes with mutation and expression data, respectively, available in both CCLE and TCGA samples were analyzed. Log-scale IC_{50} values of all cell lines in response to 265 anti-cancer

drugs were collected from the GDSC Project [7]. After imputation of missing values, the range of log IC₅₀ was from -9.8 to 12.8 with a standard deviation of 2.6 (Fig. 2a). We designed DeepDR with three building blocks: 4-layer M_{enc} and 4-layer E_{enc} for capturing high-order features and reducing dimensions of mutation and expression data, and a 5-layer prediction network P integrating the mutational and transcriptomic features to predict IC₅₀ of multiple drugs (Fig. 1). To make the best use of the large collection of TCGA pan-cancer data, we pre-trained an autoencoder for each data type and extracted the encoders, M_{enc} (number of neurons at each layer, 18,281, 1024, 256, and 64) and E_{enc} (15,363, 1024, 256, and 64), to construct our final model (detailed in Methods). Output neurons of the two encoders were linked to P (number of neurons at each layer, 64 + 64, 128, 128, 128, and 265), of which the last layer outputs predicted IC₅₀. Architecture of the complete neural networks is shown in Fig. 1b.

After pre-training M_{enc} and E_{enc} components, we trained the entire model using 80% of CCLE samples together with a validation set of 10% of samples to avoid overfitting. The remaining samples (64 cells; 16,960 cell-drug combinations) were used for testing. The model achieved an overall MSE in IC₅₀ of 1.53,

corresponding to 1.48 and 1.98 in training/validation and testing data, respectively. Generally, the distribution of predicted IC₅₀ was similar to original data (Fig. 2a-b), while the two modes of original data seemed to be enhanced (highlighted in Fig. 2a). In both training/validation and testing data, the prediction was highly consistent to the true data in terms of IC₅₀ values (Pearson correlation; ρ_P) and rank of drugs (Spearman correlation; ρ_S) of a sample ($\rho_P \in [0.70, 0.96]$, $\rho_S \in [0.62, 0.95]$, and all P -values $< 1.0 \times 10^{-29}$; Fig. 2c-d). Of note, correlations achieved in training/validation and testing samples were highly comparable (Fig. 2c-d), confirming the performance of our model.

Performance comparisons to other designs

To test the stability of DeepDR, we ran 100 training processes each of which training, validation, and testing cells were reselected. Overall, the model converged in 14.0 epochs (st. dev., 3.5; Table 1) and achieved an MSE of 1.96 in testing samples (st. dev., 0.13; Fig. 2e and Table 1). We compared the performance to linear regression, SVM, and four analog DNNs of DeepDR, including random initialization (identical architecture, but without TCGA pre-training of M_{enc} and E_{enc}), PCA (M_{enc} and E_{enc} each replaced by top 64 principal

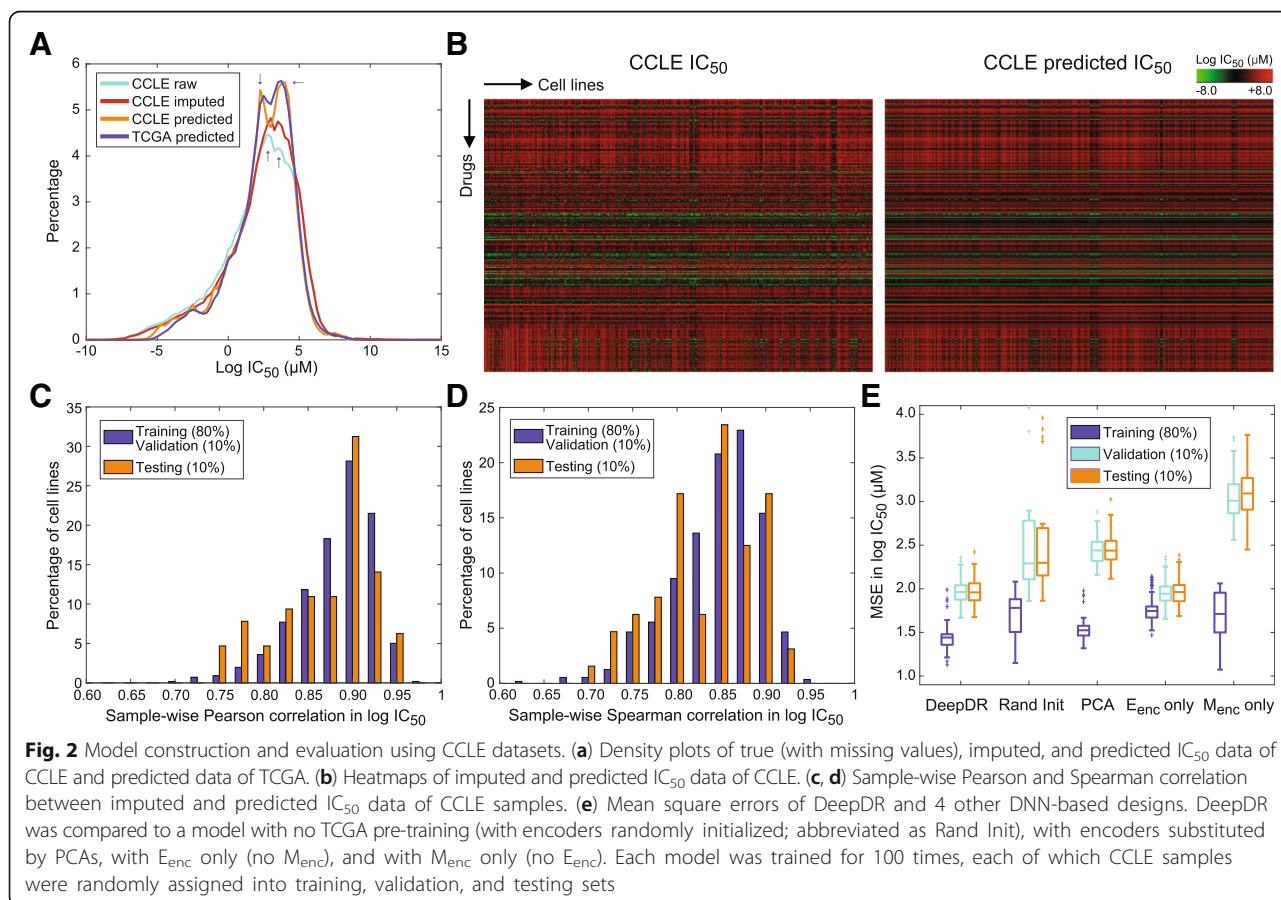


Table 1 Performance of DeepDR and other models

Measurement	DeepDR	Linear regression	SVM	Random initialization	PCA	E _{enc} only	M _{enc} only
Median MSE in testing samples ^a	1.96	10.24 ^b	8.92 ^c	2.30	2.44	1.96	3.09
Median number of training epochs ^a	14	–	–	9	29	17	9.5

^aMedian of 100 shuffles of training, validation, and testing samples

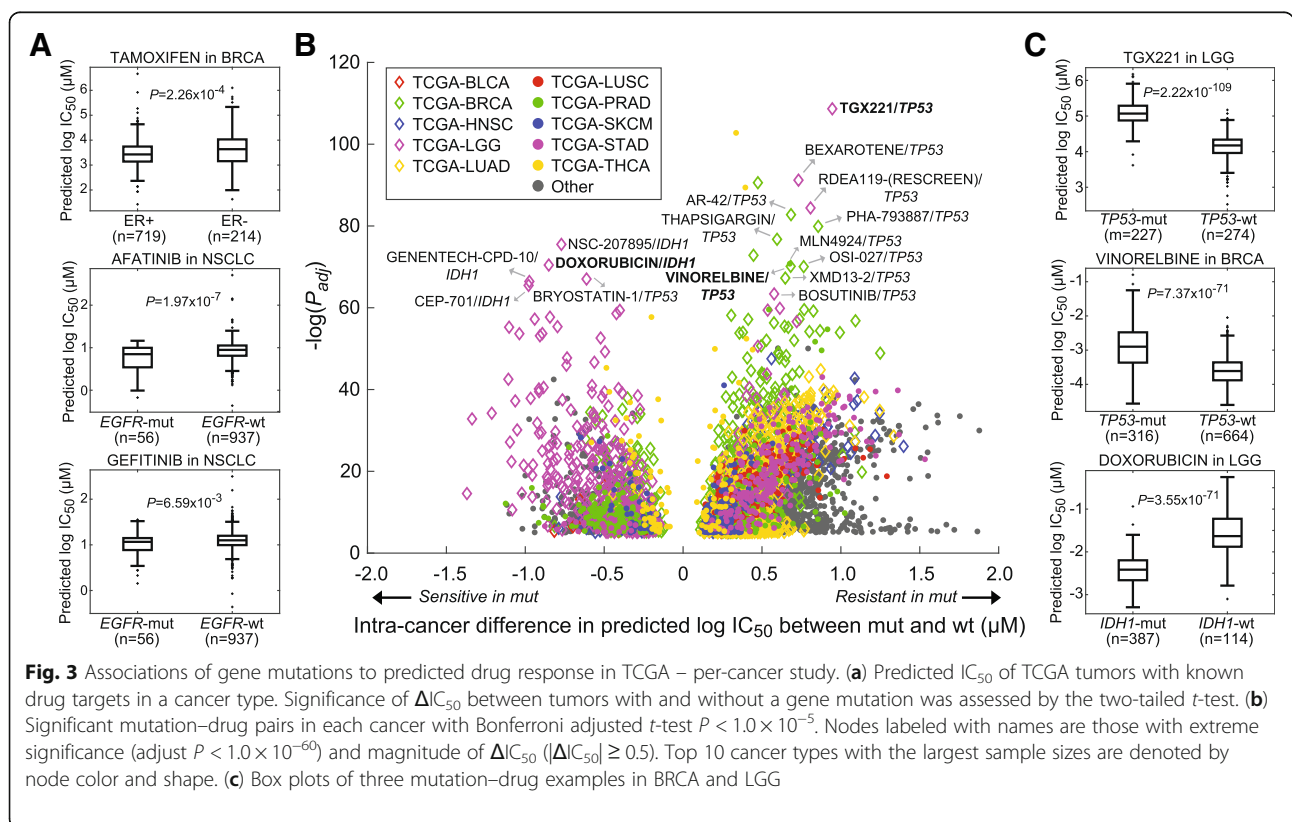
^bResult of one multivariate regression model

^cResults of 265 SVM models, each predicting IC₅₀ for a drug

components of mutation and expression data), M_{enc} only (E_{enc} removed from DeepDR), and E_{enc} only (M_{enc} removed from DeepDR). The two classical methods seemed to suffer from high MSE in testing samples (10.24 and 8.92 for linear regression and SVM, respectively; Table 1). DeepDR also outperformed DNNs with random initialization and PCA in MSE (difference in medians, 0.34 and 0.48; Fig. 2e and Table 1) and stability (st. dev. of MSE in testing samples = 0.13, 1.21, and 0.17 for DeepDR, random initialization, and PCA, respectively; Fig. 2e). While the E_{enc}-only model achieved similar performance to our model (difference in medians = 0.0042; Fig. 2E and Table 1), the addition of M_{enc} seemed to bring faster convergence (difference in medians = 3; Table 1). Our data echoed the biological premise that gene expressions are more directly linked to biological functions and thus richer in information burden than mutations.

Associations of gene mutations to predicted drug response in TCGA – Per-cancer study

In search of effective anti-cancer drugs in tumors, we applied DeepDR directly to predict the response of 9059 TCGA samples to the 265 anti-cancer drugs. The predicted IC₅₀ values followed a similar distribution to CCL6 cells (Fig. 2a, blue line). Realizing the different nature of cell lines and tumors, we started by examining several drugs with well-known target genes. As shown in Fig. 3a, breast invasive carcinoma (BRCA) with positive estrogen receptor (ER; assessed by immunohistochemistry by TCGA) responded to a selective estrogen receptor modulator, tamoxifen, significantly better than ER-negative patients (*t*-test $P = 2.3 \times 10^{-4}$). Also, two EGFR inhibitors, afatinib and gefitinib, achieved better performance in non-small cell lung cancers (NSCLC) with mutated EGFR ($P = 2.0 \times 10^{-7}$ and 6.6×10^{-3}). While the promising results on these well-characterized drugs showed the applicability of our model to tumors,



we noted that the magnitude of differences in predicted IC_{50} levels was modest, underlining the fundamental differences between cell lines and tumors. In order to prioritize mutations underlying drug response, we systematically analyzed all cancer–mutation–drug combinations and tested the significance of differences in IC_{50} between samples with and without a mutation for each cancer. Here only genes with a mutation rate higher than 10% and harbored by at least 10 patients in a cancer were analyzed. With a stringent criterion of Bonferroni-adjusted t -test $P < 1.0 \times 10^{-5}$, we identified a total of 4453 significant cancer–mutation–drug combinations involving 256 drugs and 169 cancer–mutation combinations (Fig. 3b). The top three combinations were *TP53* mutations in lung adenocarcinoma (LUAD; modulating response to 235 drugs), lung squamous cell carcinoma (LUSC; 228 drugs), and stomach adenocarcinoma (STAD; 224 drugs) (Table 2). *TP53* was one of the most frequently mutated and well-studied genes in many cancers. The mutation has been shown to be associated with cancer stem cells and resistance functions and thus regulates drug resistance [25, 26]. For instance, our data indicated its associations with resistance of a PI3K β inhibitor, TGX221, in 9 cancers including low-grade glioma (LGG; mean difference in IC_{50} (ΔIC_{50}) = 0.95; $P = 2.2 \times 10^{-109}$; Fig. 3c) and resistance of vinorelbine in BRCA (ΔIC_{50} = 0.68; $P = 7.4 \times 10^{-71}$; Fig. 3c) and 6 other cancers. We also identified gene mutations that sensitized tumors to a large number of drugs, such as *IDH1* (138 drugs; Table 2). *IDH1* was the most frequently mutated gene in LGG (77.3% in our data; Table 2) and known to regulate cell cycle of glioma cells and enhance the response to chemotherapy [27]. Our finding agreed with the report and showed that *IDH1* mutation dramatically reduced IC_{50} of chemotherapeutic agents, e.g., doxorubicin in LGG (ΔIC_{50} = -0.85; $P = 3.6 \times 10^{-71}$; Fig. 3c).

Associations of gene mutations to predicted drug response in TCGA – Pan-cancer study

We also carried out a study to explore how gene mutations affect drug response in a pan-cancer setting. The

analysis was focused on 11 genes with mutation rates higher than 10% across all TCGA samples (Table 3). Using an identical criterion, we identified 2119 significant mutation–drug pairs composed of 256 drugs, among which 1882 (88.8%) and 237 (11.2%) were more resistant and sensitive in mutated samples, respectively (Fig. 4a and Table 3). *TP53* (251 drugs), *CSMD3* (223), *SYNE1* (218), *TTN* (206), and *RYR2* (199) were the top drug response-modulating genes (Table 3). Among them, *TP53* (9 sensitive and 242 resistant drugs) and *TTN* mutations (44 and 162) were associated with the largest numbers of resistant and sensitive drugs, respectively (Table 3). Thus, we further investigated drugs associated with the 2 genes. Many of the drugs with large *TP53* mutations-modulated changes in ΔIC_{50} ($|\Delta IC_{50}| \geq 0.7$; Fig. 4a-b) were previously studied in different cancer types by in vitro models. For instance, wildtype *TP53* is required in the anti-cancer actions of CX-5461 [28, 29] and sorafenib [30] (both P of $\Delta IC_{50} \sim 0$ in our data; Fig. 4b), sensitizes various cancer cells to bortezomib [31] ($P = 4.4 \times 10^{-308}$; Fig. 4b), and enhances phenformin-induced growth inhibition and apoptosis [32] ($P = 2.0 \times 10^{-241}$; Fig. 4b). As for previously less explored *TTN* mutations, the longest gene in human genome known to carry a large number of variations, our data indicated that perhaps *TTN* acts as a marker gene of tumors sensitized to chemotherapeutic agents such as vinorelbine ($P \sim 0$; Fig. 4c) and a potential anti-cancer drug epothilone B ($P = 2.5 \times 10^{-253}$; Fig. 4c). Taken together findings from our per- and pan-cancer studies, we have demonstrated the applicability of our model to predict drug response of tumors and unveil novel and well-studied genes modulating drug response in cancer.

Pharmacogenomics analysis of docetaxel and CX-5461 in TCGA

To unveil the pharmacogenomics landscape of drugs, a comprehensive study of mutation and expression profiles associated with resistance of a drug in a pan-cancer

Table 2 Top mutations in modulating drug response among individual cancers

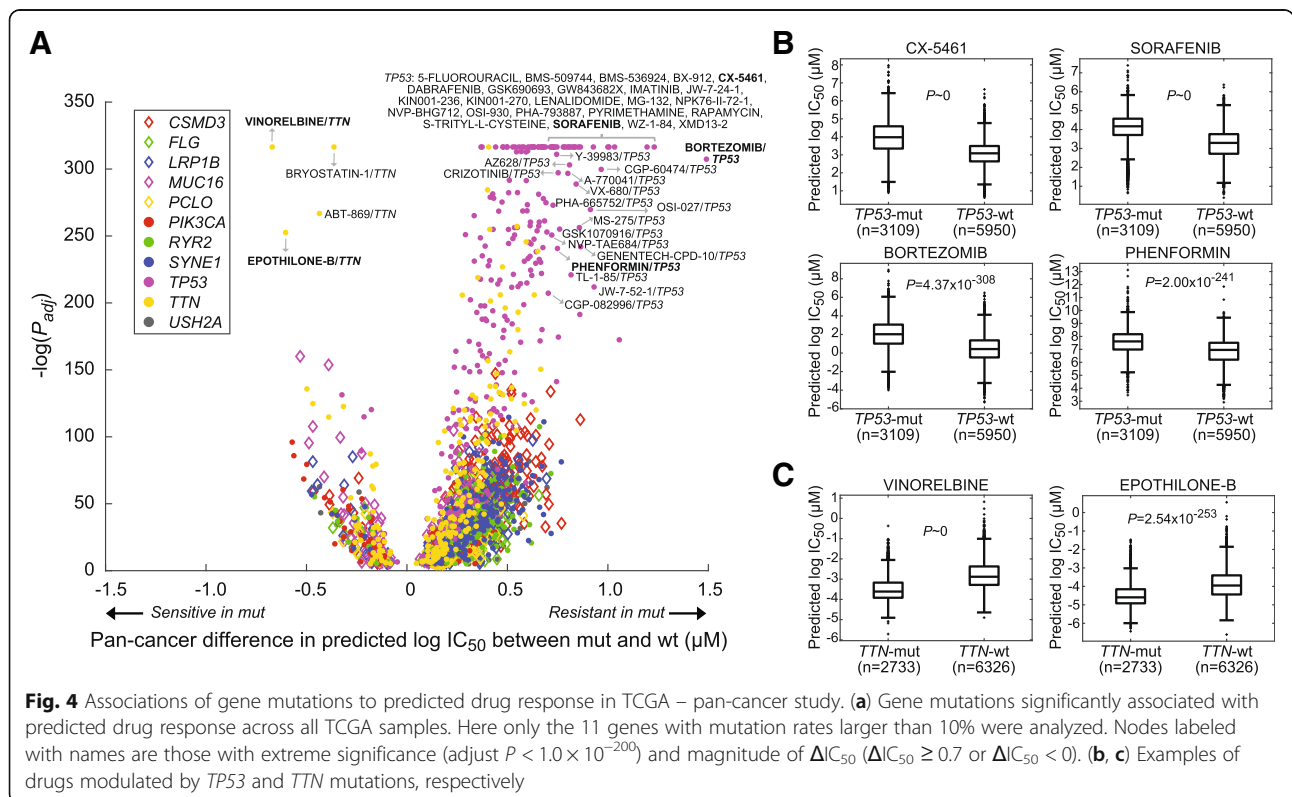
Cancer	Gene	Mutation rate	Num. modulated drugs	Num. sensitive drugs	Num. resistant drugs
LUAD	<i>TP53</i>	46.1%	235	0	235
LUSC	<i>TP53</i>	75.1%	228	0	228
STAD	<i>TP53</i>	43.3%	224	0	224
HNSC	<i>TP53</i>	66.1%	207	0	207
COAD	<i>TP53</i>	55.7%	197	0	197
LIHC	<i>TP53</i>	27.0%	194	1	193
BRCA	<i>TP53</i>	32.2%	182	7	175
LGG	<i>IDH1</i>	77.3%	159	138	21
PRAD	<i>TP53</i>	10.8%	146	1	145
KIRC	<i>PBRM1</i>	38.0%	142	3	139

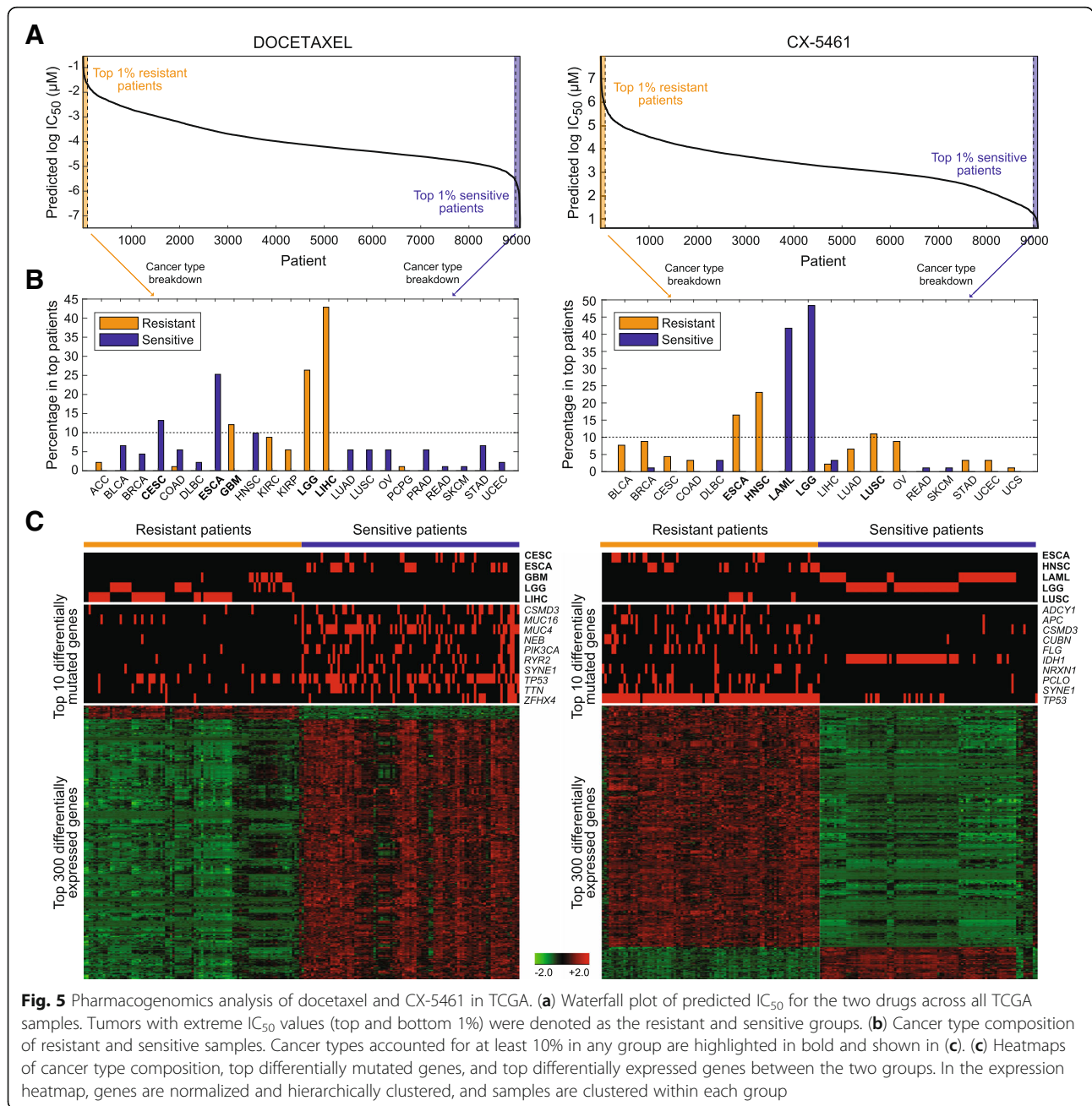
Table 3 Top gene mutations modulating pan-cancer drug response

Gene	Mutation rate	Num. modulated drugs	Num. sensitive drugs	Num. resistant drugs
TP53	34.3%	251	9	242
CSMD3	12.6%	223	12	211
SYNE1	11.5%	218	10	208
TTN	30.2%	206	44	162
RYR2	11.9%	199	14	185
USH2A	10.7%	191	12	179
LRP1B	12.1%	188	19	169
FLG	11.0%	183	9	174
MUC16	19.5%	161	51	110
PCLO	10.5%	155	12	143
PIK3CA	11.7%	144	45	99

setting was carried out. Here we took two drugs as demonstrating examples, a widely used chemotherapeutic agent docetaxel and a novel anti-cancer drug CX-5461 currently under investigation in several cancers. For each drug, pan-cancer patients predicted to be very sensitive and resistant (with IC₅₀ in bottom and top 1%, *n* = 91 in each group; Fig. 5a, left panel) were compared for cancer type compositions, mutation rates, and differential gene expression. Top cancer types of docetaxel-sensitive patients were esophageal carcinoma (ESCA; 25.3%), cervical and endocervical cancer (CESC; 13.2%), and head and neck squamous cell carcinoma (HNSC; 9.9%)

(Fig. 5b, left panel), while top resistant patients were mainly liver hepatocellular carcinoma (LIHC; 42.9%), LGG (26.4%), and glioblastoma multiforme (GBM; 12.1%) (Fig. 5b, left panel). Top 10 gene with most changed mutation rates between the two groups of patients are listed in Fig. 5c. On average, each sensitive tumor harbored 2.7 mutations among these genes, much higher than 0.51 observed in the resistant group (Fig. 5c, left panel), implying tumors with higher mutation burdens in crucial genes may be more vulnerable to the treatment. Of note, a great majority of the most significantly differentially expressed genes were upregulated in





sensitive patients (Fig. 5c, left panel). We performed functional annotation analysis of the top 300 genes in Gene Ontology terms of biological processes and molecular functions using the Database for Annotation, Visualization and Integrated Discovery (DAVID) v6.7 [33, 34]. While we did not observe any cluster of functions related to microtubule, through which docetaxel physically binds to the cell and regulate the cell cycle [35], these drug sensitivity-related genes were indeed predominantly enriched in functions governing the mitotic cell cycle (Table 4). The observation largely reflected the nature of the chemotherapeutic agent to

target highly proliferative cells and the dependence of drug response on the ability to pass cell-cycle checkpoints. In addition to docetaxel, we analyzed a novel anti-cancer agent, CX-5461. This inhibitor of ribosomal RNA synthesis has been shown with anti-cancer properties in cancer cells [36, 37] and is now under phase I/II clinical trial in solid tumors (NCT number, NCT02719977). In hematopoietic malignancies, it was recently shown to outperform standard chemotherapy regimen in treating aggressive acute myeloid leukemia (LAML) [29], and its anti-cancer effects were dependent on wild-type *TP53* [28, 29]. Concordantly, in our data,

Table 4 Top GO clusters enriched in top 300 differentially expressed genes associated with predicted response to docetaxel

GO ID	GO term	Num. genes	P-value
Cluster 1 (enrichment score: 10.89)			
GO:0007049	cell cycle	40	1.13×10^{-10}
GO:0022402	cell cycle process	33	3.51×10^{-10}
GO:0000279	M phase	32	1.01×10^{-15}
Cluster 2 (enrichment score: 3.96)			
GO:0000166	nucleotide binding	56	1.95×10^{-4}
GO:0032553	ribonucleotide binding	54	2.74×10^{-6}
GO:0032555	purine ribonucleotide binding	54	2.74×10^{-6}
Cluster 3 (enrichment score: 3.45)			
GO:0000278	mitotic cell cycle	26	1.01×10^{-9}
GO:0051726	regulation of cell cycle	15	8.48×10^{-4}
GO:0007346	regulation of mitotic cell cycle	12	3.09×10^{-5}
Cluster 4 (enrichment score: 2.47)			
GO:0051327	M phase of meiotic cell cycle	8	9.46×10^{-4}
GO:0007126	meiosis	8	9.46×10^{-4}
GO:0051321	meiotic cell cycle	8	1.07×10^{-3}
Cluster 5 (enrichment score: 2.07)			
GO:0051276	chromosome organization	13	8.64×10^{-2}
GO:0007059	chromosome segregation	6	9.34×10^{-3}
GO:0000070	mitotic sister chromatid segregation	5	2.45×10^{-3}

Each cluster is represented by the largest three GO terms

Table 5 Top GO clusters enriched in top 300 differentially expressed genes associated with predicted response to CX-5461

GO ID	GO term	Num. genes	P-value
Cluster 1 (enrichment score: 8.65)			
GO:0043062	extracellular structure organization	17	2.93×10^{-9}
GO:0030198	extracellular matrix organization	15	4.55×10^{-10}
GO:0005201	extracellular matrix structural constituent	13	2.64×10^{-9}
Cluster 2 (enrichment score: 6.13)			
GO:0008544	epidermis development	18	2.35×10^{-9}
GO:0007398	ectoderm development	18	7.71×10^{-9}
GO:0030855	epithelial cell differentiation	8	4.60×10^{-3}
Cluster 3 (enrichment score: 4.23)			
GO:0030199	collagen fibril organization	9	7.34×10^{-9}
GO:0032963	collagen metabolic process	6	5.37×10^{-5}
GO:0044259	multicellular organismal macromolecule metabolic process	6	8.96×10^{-5}
Cluster 4 (enrichment score: 2.84)			
GO:0006928	cell motion	18	8.22×10^{-4}
GO:0016477	cell migration	13	9.51×10^{-4}
GO:0048870	cell motility	13	2.33×10^{-3}
Cluster 5 (enrichment score: 2.60)			
GO:0060429	epithelium development	12	6.39×10^{-4}
GO:0030855	epithelial cell differentiation	8	4.60×10^{-3}
GO:0009913	epidermal cell differentiation	6	4.49×10^{-3}

Each cluster is represented by the largest three GO terms

LAML and lymphoid neoplasm diffuse large B-cell lymphoma (DLBC) jointly accounted for 45.1% (41.8 and 3.3%) of patients predicted to respond extremely well to CX-5461 (Fig. 5a-b, right panels). Of note, LGG comprised another 48.4% of the sensitive tumors (Fig. 5b, right panel). Nine of the top 10 differentially mutated genes were enriched in the resistant group and led by *TP53* mutations (mutation rate, 95.6% in resistant vs. 13.2% in sensitive patients; Fig. 5c, right panel), echoing data from our pan-cancer analysis (Fig. 4a-b) and previous in vitro and in vivo investigations [28, 29]. *IDH1* was the only gene preferentially mutated in sensitive tumors and largely marked LGG (mutated in 42 of 44 sensitive LGG; Fig. 5c, right panel). DAVID analysis of the top 300 differentially expressed genes highlighted differential mechanisms between solid and non-solid tumors, such as extracellular matrix and cell motion (Table 5). Altogether, the pharmacogenomics analyses revealed well-known resistance mechanisms of docetaxel and shed light on the potential of CX-5461 on hematopoietic malignancies and LGG.

Discussion

DNN is unquestionably one of the largest computational breakthroughs in the era of big data. Although promising results of our and other studies have demonstrated its ability of solving challenging bioinformatic tasks, the method has several fundamental limitations. For instance, due to high representational power and model complexity, the method suffers from overfitting and the requirement of large training data. Addressing this, the present study adopts a training-validation partition of training data to allow early stopping to the training process [38]. Future work may further incorporate dropout and regularization to DNNs. Also, by taking advantage of the transferability of neural networks, we used the huge volume of TCGA data to equip our model the ability of capturing representations of mutation and expression data. Transferring the learned parameters to initialize our model virtually increased the sample size of our training data. Our data from 100 iterations of model training suggest the stability of performance and insensitivity to the selection of training samples. With the availability of more large-scale drug screening data, we expect the proposed model to make even more accurate predictions and unveil subtle pharmacogenomics features. Furthermore, DeepDR may incorporate additional genomic mutation information, such as copy number alterations, into data matrices M^{TCGA} and M^{CCLE} , to enrich the complexity of tumor mutation for model training and further reduce the training MSE. Because of the nature of DNNs as black boxes, the interpretability of results is typically limited. In this study, by integrating genomics profiles to the predictions, we systematically

investigated how single gene mutations, as well as the interplay between cancer type, mutations, and biological functions, were associated with the predicted drug response. Several novel methods were recently proposed to extract features learned by neural networks, such as network-centric approach [39] and decomposition of predicted outputs by backpropagation onto specific input features [40] (reviewed in [41]). Future works may incorporate these methods to provide a landscape of pharmacogenomics and further reveal novel oncogenic genomics profiles.

Conclusions

This study addresses the need for a translation of pharmacogenomics features identified from pre-clinical cell line models to predict drug response of tumors. We developed a DNN model capable of extracting representative features of mutations and gene expression, and bridging knowledge learned from cancer cell lines and applications to tumors. We showed the reliability of the model and its superior performance than four different methods. Applying our model to the TCGA collection of tumors, we identified both well-studied and novel resistance mechanisms and drug targets. Overall, the proposed model is widely applicable to incorporate other omics data and to study a wider range of drugs, paving the way to the realization of precision oncology.

Abbreviations

ACC: adrenocortical cancer; BLCA: bladder urothelial carcinoma; BRCA: breast invasive carcinoma; CCLE: Cancer Cell Line Encyclopedia; CESC: cervical and endocervical cancer; CHOL: cholangiocarcinoma; COAD: colon adenocarcinoma; DL: deep learning; DLBC: diffuse large B-cell lymphoma; DNN: deep neural network; E_{enc} : expression encoder; ER: estrogen receptor; ESCA: esophageal carcinoma; GBM: glioblastoma multiforme; HNSC: head and neck squamous cell carcinoma; IC_{50} : half maximal inhibitory concentration; KICH: kidney chromophobe; KIRC: kidney clear cell carcinoma; KIRP: kidney papillary cell carcinoma; LAML: acute myeloid leukemia; LGG: lower grade glioma; LIHC: liver hepatocellular carcinoma; LUAD: lung adenocarcinoma; LUSC: lung squamous cell carcinoma; M_{enc} : mutation encoder; MESO: mesothelioma; MSE: mean squared error; MUT: mutated; NSCLC: non-small cell lung cancer; Num: number; OV: ovarian serous cystadenocarcinoma; P: prediction network; P : P -value; PCA: principal component analysis; PCPG: pheochromocytoma and paraganglioma; PRAD: prostate adenocarcinoma; Rand Init: random initialization; READ: Rectum adenocarcinoma; SARC: Sarcoma; SKCM: Skin cutaneous melanoma; STAD: Stomach adenocarcinoma; SVM: Support vector machine; TCGA: The Cancer Genome Atlas; TGCT: Testicular germ cell tumor; THCA: Thyroid carcinoma; THYM: Thymoma; UCEC: Uterine corpus endometrioid carcinoma; UCS: Uterine carcinosarcoma; UVM: Uveal melanoma; WT: Wildtype

Acknowledgements

The authors greatly appreciate the brilliant and constructive inputs from reviewers and participants of the International Conference on Intelligent Biology and Medicine (ICIBM 2018).

Availability of data and material

The dataset supporting the conclusions of this article is included within the article.

Funding

This research and this article's publication costs were supported partially by the NCI Cancer Center Shared Resources (NIH-NCI P30CA54174 to YC), NIH (CTSA 1UL1RR025767-01 to YC, and R01GM113245 to YH), CPRIT (RP160732 to YC), and San Antonio Life Science Institute (SALSI Innovation Challenge Award 2016 to YH and YC and SALSI Postdoctoral Research Fellowship to YCC). The funding sources had no role in the design of the study and collection, analysis, and interpretation of data and in writing the manuscript.

About this supplement

This article has been published as part of *BMC Medical Genomics Volume 12 Supplement 1, 2019: Selected articles from the International Conference on Intelligent Biology and Medicine (ICIBM) 2018: medical genomics*. The full contents of the supplement are available online at <https://bmcmedgenomics.biomedcentral.com/articles/supplements/volume-12-supplement-1>.

Authors' contributions

All of the authors conceived the study. YCC, YH, and YC designed the model. YCC performed data analysis. YCC, YH, and YC interpreted the data. YCC, YH, and YC wrote the manuscript. All of the authors have read and approved the final manuscript.

Ethics approval and consent to participate

Not applicable.

Consent for publication

Not applicable.

Competing interests

The authors declare that they have no competing interests.

Publisher's Note

Springer Nature remains neutral with regard to jurisdictional claims in published maps and institutional affiliations.

Author details

¹Greehey Children's Cancer Research Institute, University of Texas Health Science Center at San Antonio, San Antonio, TX 78229, USA. ²Department of Electrical and Computer Engineering, The University of Texas at San Antonio, San Antonio, TX 78249, USA. ³Laboratory of Information Fusion Technology of Ministry of Education, School of Automation, Northwestern Polytechnical University, Xi'an 710072, Shaanxi, China. ⁴Department of Epidemiology and Biostatistics, University of Texas Health Science Center at San Antonio, San Antonio, TX 78229, USA.

Published: 31 January 2019

References

- Hanahan D, Weinberg RA. Hallmarks of cancer: the next generation. *Cell*. 2011;144(5):646–74.
- Schmitt MW, Loeb LA, Salk JJ. The influence of subclonal resistance mutations on targeted cancer therapy. *Nat Rev Clin Oncol*. 2016;13(6):335–47.
- Phillips KA, Veenstra DL, Oren E, Lee JK, Sadee W. Potential role of pharmacogenomics in reducing adverse drug reactions: a systematic review. *JAMA : the journal of the American Medical Association*. 2001; 286(18):2270–9.
- Hertz DL, Rae J. Pharmacogenetics of cancer drugs. *Annu Rev Med*. 2015;66:65–81.
- Mina M, Raynaud F, Tavernari D, Battistello E, Sungalee S, Saghafia S, Laessle T, Sanchez-Vega F, Schultz N, Oricchio E, et al. Conditional selection of genomic alterations dictates cancer evolution and oncogenic dependencies. *Cancer Cell*. 2017;32(2):155–68 e156.
- Park S, Lehner B. Cancer type-dependent genetic interactions between cancer driver alterations indicate plasticity of epistasis across cell types. *Mol Syst Biol*. 2015;11(7):824.
- Iorio F, Knijnenburg TA, Vis DJ, Bignell GR, Menden MP, Schubert M, Aben N, Goncalves E, Barthorpe S, Lightfoot H, et al. A landscape of Pharmacogenomic interactions in Cancer. *Cell*. 2016;166(3):740–54.
- Yang W, Soares J, Greninger P, Edelman EJ, Lightfoot H, Forbes S, Bindal N, Beare D, Smith JA, Thompson IR, et al. Genomics of drug sensitivity in Cancer (GDSC): a resource for therapeutic biomarker discovery in cancer cells. *Nucleic Acids Res*. 2013;41(Database issue):D955–61.
- Alipanahi B, Delong A, Weirauch MT, Frey BJ. Predicting the sequence specificities of DNA- and RNA-binding proteins by deep learning. *Nat Biotechnol*. 2015;33(8):831–8.
- Zhou J, Troyanskaya OG. Predicting effects of noncoding variants with deep learning-based sequence model. *Nat Methods*. 2015;12(10):931–4.
- Lin C, Jain S, Kim H, Bar-Joseph Z. Using neural networks for reducing the dimensions of single-cell RNA-Seq data. *Nucleic Acids Res*. 2017;45(17):e156.
- Angermueller C, Lee HJ, Reik W, Stegle O. DeepCpG: accurate prediction of single-cell DNA methylation states using deep learning. *Genome Biol*. 2017; 18(1):67.
- Chaudhary K, Poirion OB, Lu L, Garmire LX. Deep learning-based multi-omics integration robustly predicts survival in liver Cancer. *Clinical cancer research: an official journal of the American Association for Cancer Research*. 2018;24(6):1248–59.
- Wen M, Zhang Z, Niu S, Sha H, Yang R, Yun Y, Lu H. Deep-learning-based drug-target interaction prediction. *J Proteome Res*. 2017;16(4):1401–9.
- Kadurin A, Aliper A, Kazennov A, Mamoshina P, Vanhaelen Q, Khrabrov K, Zhavoronkov A. The cornucopia of meaningful leads: applying deep adversarial autoencoders for new molecule development in oncology. *Oncotarget*. 2017;8(7):10883–90.
- Preuer K, Lewis RPI, Hochreiter S, Bender A, Bulusu KC, Klambauer G. DeepSynergy: predicting anti-cancer drug synergy with deep learning. *Bioinformatics*. 2018;34(9):1538–46.
- Patro R, Duggal G, Love MI, Irizarry RA, Kingsford C. Salmon provides fast and bias-aware quantification of transcript expression. *Nat Methods*. 2017; 14(4):417–9.
- Newton W, Novak AM, Swatloski T, McColl DC, Chopra S, Graim K, Weinstein AS, Baertsch R, Salama SR, Ellrott K, et al. TumorMap: exploring the molecular similarities of Cancer samples in an interactive portal. *Cancer Res*. 2017;77(21):e111–4.
- Barretina J, Caponigro G, Stransky N, Venkatesan K, Margolin AA, Kim S, Wilson CJ, Lehár J, Kryukov GV, Sonkin D, et al. The Cancer cell line encyclopedia enables predictive modelling of anticancer drug sensitivity. *Nature*. 2012;483(7391):603–7.
- Cancer Cell Line Encyclopedia C. Genomics of drug sensitivity in Cancer C: Pharmacogenomic agreement between two cancer cell line data sets. *Nature*. 2015;528(7580):84–7.
- Kowarik A, Templ M. Imputation with the R Package VIM. *Journal of Statistical Software*. 2016;74(7):1–16.
- Alfons A, Templ M. Estimation of Social Exclusion Indicators from Complex Surveys. *The R Package laeken 2013*. 2013;54(15):25.
- He K, Zhang X, Ren S, Sun J. Delving deep into rectifiers: surpassing human-level performance on imagenet classification. *Proceedings of the IEEE international conference on computer vision*. 2015;2015:1026–34.
- Pumperla M. Keras + Hyperopt: A very simple wrapper for convenient hyperparameter optimization. 2016.
- Shetzer Y, Solomon H, Koifman G, Molchadsky A, Horesh S, Rotter V. The paradigm of mutant p53-expressing cancer stem cells and drug resistance. *Carcinogenesis*. 2014;35(6):1196–208.
- Hientz K, Mohr A, Bhakta-Guha D, Efferth T. The role of p53 in cancer drug resistance and targeted chemotherapy. *Oncotarget*. 2017;8(5):8921–46.
- Wang JB, Dong DF, Wang MD, Gao K. IDH1 overexpression induced chemotherapy resistance and IDH1 mutation enhanced chemotherapy sensitivity in glioma cells in vitro and in vivo. *Asian Pac J Cancer Prev*. 2014; 15(1):427–32.
- Bywater MJ, Poortinga G, Sanij E, Hein N, Peck A, Cullinane C, Wall M, Cluse L, Drygin D, Anderes K, et al. Inhibition of RNA polymerase I as a therapeutic strategy to promote cancer-specific activation of p53. *Cancer Cell*. 2012;22(1):51–65.
- Hein N, Cameron DP, Hannan KM, Nguyen NN, Fong CY, Sornkom J, Wall M, Pavy M, Cullinane C, Diesch J, et al. Inhibition of pol I transcription treats murine and human AML by targeting the leukemia-initiating cell population. *Blood*. 2017;129(21):2882–95.
- Wei JC, Meng FD, Qu K, Wang ZX, Wu QF, Zhang LQ, Pang Q, Liu C. Sorafenib inhibits proliferation and invasion of human hepatocellular carcinoma cells via up-regulation of p53 and suppressing FoxM1. *Acta Pharmacol Sin*. 2015;36(2):241–51.
- Ling X, Calinski D, Chanan-Khan AA, Zhou M, Li F. Cancer cell sensitivity to bortezomib is associated with survivin expression and p53 status but not cancer cell types. *J Exp Clin Cancer Res*. 2010;29:8.

32. Li P, Zhao M, Parris AB, Feng X, Yang X. p53 is required for metformin-induced growth inhibition, senescence and apoptosis in breast cancer cells. *Biochem Biophys Res Commun.* 2015;464(4):1267–74.
33. Huang d W, Sherman BT, Lempicki RA. Systematic and integrative analysis of large gene lists using DAVID bioinformatics resources. *Nat Protoc.* 2009;4(1):44–57.
34. Huang d W, Sherman BT, Lempicki RA. Bioinformatics enrichment tools: paths toward the comprehensive functional analysis of large gene lists. *Nucleic Acids Res.* 2009;37(1):1–13.
35. Fulton B, Spencer CM. Docetaxel. A review of its pharmacodynamic and pharmacokinetic properties and therapeutic efficacy in the management of metastatic breast cancer. *Drugs.* 1996;51(6):1075–92.
36. Drygin D, Lin A, Bliesath J, Ho CB, O'Brien SE, Proffitt C, Omori M, Haddach M, Schwaebe MK, Siddiqui-Jain A, et al. Targeting RNA polymerase I with an oral small molecule CX-5461 inhibits ribosomal RNA synthesis and solid tumor growth. *Cancer Res.* 2011;71(4):1418–30.
37. Xu H, Di Antonio M, McKinney S, Mathew V, Ho B, O'Neil NJ, Santos ND, Silvester J, Wei V, Garcia J, et al. CX-5461 is a DNA G-quadruplex stabilizer with selective lethality in BRCA1/2 deficient tumours. *Nat Commun.* 2017;8:14432.
38. Angermueller C, Parnamaa T, Parts L, Stegle O. Deep learning for computational biology. *Mol Syst Biol.* 2016;12(7):878.
39. Yosinski J, Clune J, Nguyen A, Fuchs T, Lipson H. Understanding neural networks through deep visualization. In: *arXiv preprint arXiv:150606579*; 2015.
40. Shrikumar A, Greenside P, Kundaje A. Learning important features through propagating activation differences. In: *arXiv preprint arXiv:170402685*; 2017.
41. Kalinin AA, Higgins GA, Reamaroon N, Sorousmehr S, Allyn-Feuer A, Dinov ID, Najarian K, Athey BD. Deep learning in pharmacogenomics: from gene regulation to patient stratification. In: *arXiv preprint arXiv:180108570*; 2018.

Ready to submit your research? Choose BMC and benefit from:

- fast, convenient online submission
- thorough peer review by experienced researchers in your field
- rapid publication on acceptance
- support for research data, including large and complex data types
- gold Open Access which fosters wider collaboration and increased citations
- maximum visibility for your research: over 100M website views per year

At BMC, research is always in progress.

Learn more biomedcentral.com/submissions

